INTER-NOISE 2006

3-6 DECEMBER 2006
HONOLULU, HAWAII, USA

An Evaluation of Hand-Arm System Models Used for Vibrating Tool Analyses and Test Rig Constructions

Ren G. Dong, Daniel E. Welcome, John Z. Wu, and Thomas W. McDowell
National Institute for Occupational Safety and Health
Engineering & Control Technology Branch
1095 Willowdale Road
Morgantown, West Virginia 26505, USA

ABSTRACT

Many biodynamic model structures or configurations of the hand-arm system have been proposed. The objectives of this study are to introduce a new model, to redefine the parameters of three typical models using newly published experimental data, and to assess their usefulness for vibration tool analyses and test rig constructions. To achieve these objectives, the traditional 2-DOF, 3-DOF, and 4-DOF and one new model proposed by the authors were used. The biodynamic responses to hand-transmitted vibration measured at the hand driving-point under a combined grip and push action were used to determine the parameters of the models using a least root-mean-square error curve fitting method. This study found that the new model and the 3-DOF and 4-DOF models fit the experimental impedance data extremely well. When judged using apparent mass, the 2-DOF model also fits the experimental data well . The natural frequencies and damping ratios resulting from these models are in reasonable ranges. The relative static deformations of these models are also acceptable for test rig construction. This study concluded that the new model provides the best choice for analyzing tools and for constructing hand-arm simulators. However, if the hand-tool dynamic interactions below 100 Hz are of major concern, the 2-DOF model is simpler and less expensive for the construction of a hand-arm simulator.

1 INTRODUCTION

The biodynamic response of the hand-arm system is one of the important foundations for understanding mechanisms of vibration-induced disorders and for developing better standards for assessing vibration exposure risks (Griffin, 1994; Dong et al., 2001). Knowledge of the biodynamic responses is required for designing and assessing vibration isolation methods and for developing hand-arm simulators for analysis and test of powered hand tools. Many analytical models with different configurations or structures have been developed. However, recent studies have identified many problems in the reported models (Rakheja et al., 2002), including those recommended in ISO10068 (1998). Some significant errors have also been identified in the reported experimental data that were used to construct the models (Dong et al., 2006). It is unclear whether the problems with these models are due to inappropriate model structures, to experimental data errors, or to both of these sources.

Therefore, the objectives of this study are to redefine the parameters of the typical traditional models using recently published experimental data, to introduce a new model, and to evaluate the usefulness of these models, especially for vibration tool analyses and hand-arm simulator construction.

2 METHODS

2.1 Model configurations

Figure 1 illustrates basic structures of the hand-arm system with the hand gripping a cylindrical handle. Based on the flexibility of the anatomical structures and the hand grip posture, the hand-arm system can be roughly divided into five parts: fingers, the remaining hand structures, forearm, upper arm, and shoulder. The upper arm and shoulder may or may not effectively participate in the response, depending mainly on the vibration frequency, arm posture, and applied hand forces. For different purposes, many models of the system have been configured and used (Dong et al., 2001; Rakheja et al., 2002).

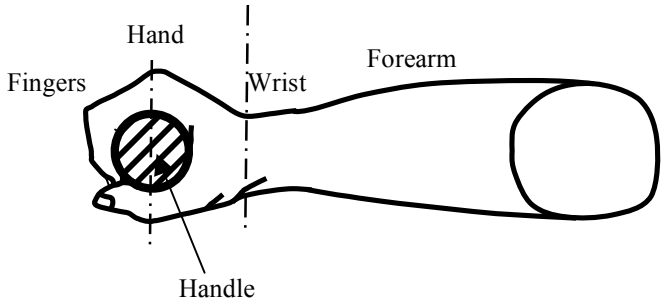

Figure 1: Basic structures of the hand-arm system and the hand power grip posture

Figure 2 shows the four typical models used in the present study. The first model (Figure 2a) is a new one. This model has two connections to the handle of a tool, respectively at the fingers and the palm of the hand. In terms of the number of mass elements in the model, it is a four degrees-of-freedom (DOF) model. M_1 and M_3 represent the masses of the contact skin for the fingers and palm, respectively. Because these two mass elements are fixed to the handle, this model actually has only two degrees-of-freedom. One of the two DOFs is the effective mass of the remaining finger structures (M_2). The second DOF is the effective mass of the remaining hand and the forearm that are lumped together and represented with M_4. Four sets of linear spring-damping elements are used to link these mass elements together and to the body or ground, which forms the new system model.

The remaining three models have typical traditional configurations that were widely used in previous studies (Rakheja et al., 2002). The parts of these models were intended to roughly represent anatomical structures of the hand-arm system, as shown in the Figure 2(b)-(d). The 3-DOF and 4-DOF models are included in ISO 10068 (1998). Similar to the new model, the hand contact skin is considered as rigid mass fixed to the handle in these three models. Different from the new model, all the traditional models have only one connection with the handle; this characteristic ignores the flexibility of the fingers relative to the remaining hand structures.

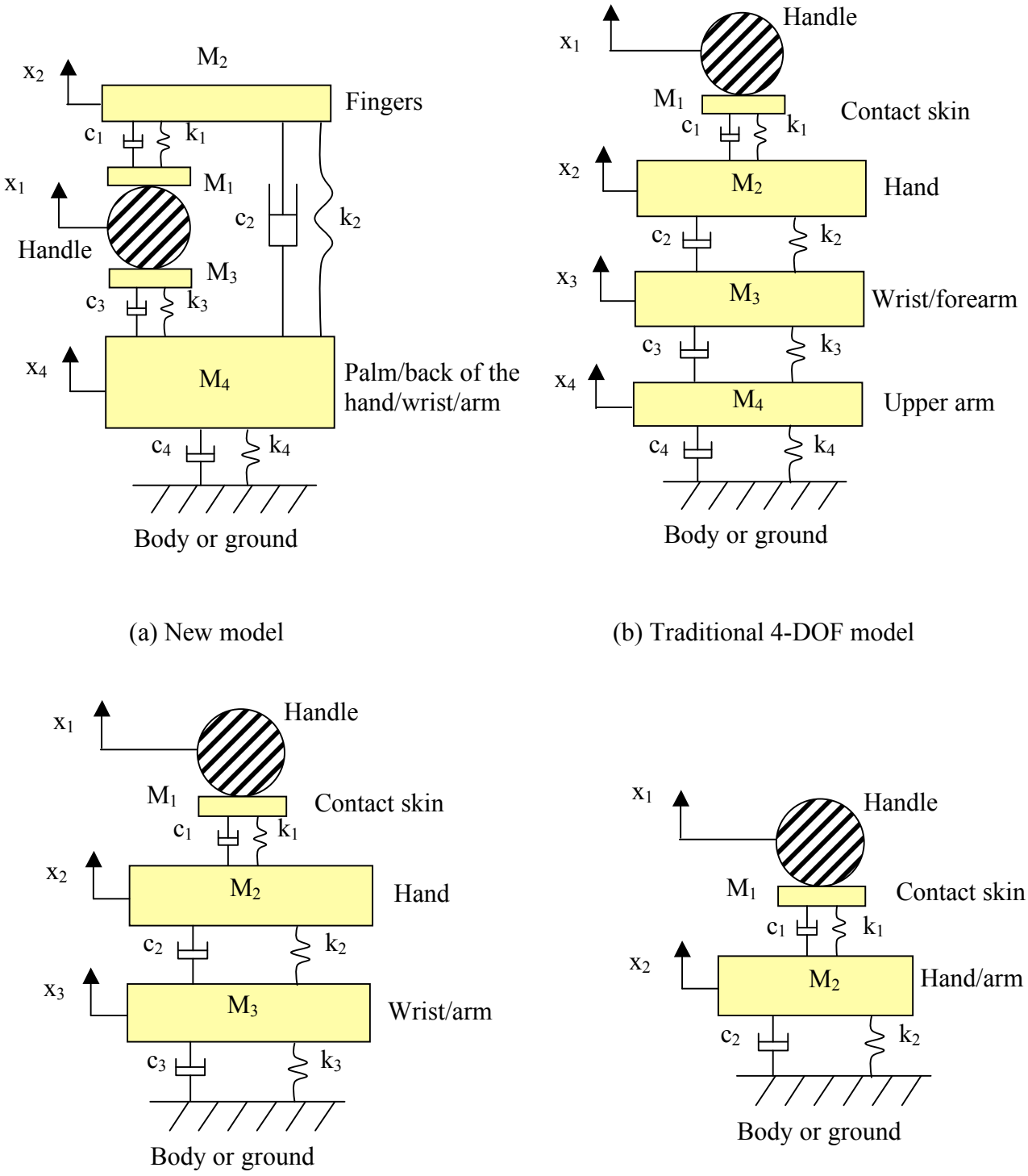

Figure 2: Four typical models of the hand-arm system

2.2 Calculation of Biodynamic Responses

The equations of motions for these models can be derived from their configurations shown in Figure 2, and they can be generally expressed as follows:

$$[M]\{\ddot{x}\}+[C]\{\dot{x}\}+[K]\{x\}=\{F\} \tag{1}$$

where *[M]* is mass matrix, *[C]* is damping matrix, *[K]* is stiffness matrix, *{F}* is force vector.

The equations of motion for the models are used to compute the dynamic forces developed at the fingers ($F_{Fingers}$), palm (F_{Palm}), and hand (F_{hand}), due to displacement (y) of the handle. The driving-point biodynamic response (DPBR) is characterized in terms of mechanical impedance (MI) at the fingers- and palm-handle interfaces on the new model or the hand-handle interface on the traditional models. Representing excitation as $y = Ye^{j\omega t}$, the distributed impedance response at the fingers ($Z_{Fingers}$) and that at the palm (Z_{Palm}) on the new model are derived from:

$$\begin{aligned} Z_{Fingers} &= \frac{F_{Fingers}}{V} = \frac{(k_1 + c_1 j\omega)(Y - X_2)}{j\omega Y} + M_1 j\omega \\ Z_{Palm} &= \frac{F_{Palm}}{V} = \frac{(k_3 + c_3 j\omega)(Y - X_4)}{j\omega Y} + M_3 j\omega \end{aligned} \tag{2}$$

where $V = j\omega Y$ is the handle velocity corresponding to excitation frequency ω, and X_2 and X_4 are the magnitudes of displacement responses of M_2 and M_4, respectively. The MI of the entire hand-arm (Z_{Hand}) on the new model is computed from:

$$Z_{Hand} = \frac{F_{Hand}}{V} = \frac{F_{Fingers} + F_{Palm}}{V} = Z_{Fingers} + Z_{Palm} \tag{3}$$

The impedance on the hand for the three traditional models is derived from:

$$Z = \frac{F_{Hand}}{V} = \frac{(k_1 + c_1 j\omega)(Y - X_2)}{j\omega Y} + M_1 j\omega \tag{4}$$

The vibration transmissibility is calculated from:

$$T_i = \frac{\ddot{X}_i}{\ddot{Y}} \tag{5}$$

The vibration power absorption flowing into the hand arm system is calculated from:

$$P = \frac{1}{2} Re(Z) \cdot |V|^2 \tag{6}$$

where *Re(Z)* is the real component of the impedance.

The vibration power flowing into the system must be equal to the sum of the vibration power dissipations distributed on all the damping elements. On each damping element, the dissipated power is calculated from:

$$P_{ci} = \frac{1}{2} c_i \Delta V_i^2 \tag{7}$$

where ΔV_i is the relative velocity between two bodies. In the calculation of the power absorption, the vibration velocity on the handle was assumed to be 0.1 m/s at each frequency.

2.3 Determination of model parameters

The measured responses reported by Dong et al. (2005) are used in this study. They were measured with six subjects with their hand and arm posture similar to that specified in ISO10819 (1996). A 40 mm split instrumented handle was used to separately measure the responses distributed at the fingers and the palm of the hand subjected to a sinusoidal vibration. Ten discrete frequencies in the 16 to 1000 Hz range were used. For the purposes of this study, the data measured under the combined 50 N grip and 50 N push were used.

The parameters of the models were determined by minimizing the rms deviations (Δ) between the predicted MI and the experimental data, termed as the error function $E(\chi)$:

for the new model,

$$E(\chi) = Re\left[\Delta Z_{Fingers}(j\omega)\right] + Im\left[\Delta Z_{Fingers}(j\omega)\right] + Re\left[\Delta Z_{palm}(j\omega)\right] + Im\left[\Delta Z_{palm}(j\omega)\right], \quad (8)$$

for the traditional 3-DOF and 4-DOF models,

$$E(\chi) = Re\left[\Delta Z_{Hand}(j\omega)\right] + Im\left[\Delta Z_{Hand}(j\omega)\right] \quad (9)$$

where '*Re*' and '*Im*' designate the real and imaginary components of impedance, respectively; $\Delta Z_{Fingers}$ and ΔZ_{Palm} are the deviations between the predicted and measured MI distributed at the fingers and palm, respectively, corresponding to excitation frequency ω; and χ is the vector of design parameters of each model (Figs. 2 and 3).

It is impossible to use the 2-DOF model to accurately simulate high frequency (>100 Hz) impedance responses. However, for the analyses and tests of some tools, such a model may be sufficient. To emphasize lower frequency responses, the apparent mass (AM), instead of the impedance, was used to determine the parameters of this model. The error function is expressed as follows:

$$E(\chi) = Re\left[\Delta AM_{Hand}(j\omega)\right] + Im\left[\Delta AM_{Hand}(j\omega)\right] \quad (7)$$

The parameter identification process was performed with the following constraints: $M_i \geq 0.$; $k_i \geq 0.$; $c_i \geq 0$. An iterative algorithm was developed to minimize $E(\chi)$ by varying each parameter in a sequential manner, while the others were held at their last updated values. An iteration cycle was completed when all the parameters were updated; convergence was considered to occur when the difference between the error magnitudes in two consecutive cycles approached a target value (for IM: < 0.01 N·s/m; for AM: < 0.01 g). The identification process was repeated by considering more than five different initial vectors. All trials converged to similar solutions suggesting uniqueness of the solution.

3 RESULTS

3.1 Model parameters and fitting results

Table 1 lists the parameters identified for the models, together with their natural frequencies and damping ratios. The total skin mass resulting from the new model (14.0 + 26.7 = 40.7 g) is

similar to that of the 3-DOF model (39.1 g) or the 4-DOF model (39.2 g). These three skin mass values are slightly less than the skin mass of the 2-DOF model (49.3 g). The total mass of the new, 2-DOF, and 3-DOF models are similar. The parameters of the 3-DOF model are also similar to those of the 4-DOF model, except those related to the additional DOF elements on the 4-DOF model. The first resonance frequencies and damping ratios of the new, 2-DOF, and 3-DOF models are similar. The highest resonance frequencies and damping ratios of the 3-DOF and 4-DOF are similar, which are larger than those of the new model. The palm contact stiffness (k3) of the new model is comparable with the k1 value of the 2-DOF model, and the k2 values of the 3-DOF and 4-DOF models. The hand contact stiffness (k1) values of the 3-DOF and 4-DOF models are similar, but they are much larger than the finger contact stiffness values of the new model.

Table 1: Comparisons of the parameters of the four models

Parameter	Units	Model			
		New	2-DOF	3-DOF	4-DOF
M_1	Kg	0.0140	0.0493	0.0391	0.0392
M_2	Kg	0.0820	1.5546	0.1487	0.1485
M_3	Kg	0.0267		1.3718	1.2354
M_4	Kg	1.4150			3.7697
k_1	N/m	207,964	62,804	450,960	452,379
k_2	N/m	6,523	4,279	68,924	73,254
k_3	N/m	58,555		3,545	567
k_4	N/m	4,206			96,623
c_1	N ·s/m	120.8	192.9	245.7	244.0
c_2	N ·s/m	37.9	76.1	190.3	187.2
c_3	N ·s/m	118.3		80.2	111.3
c_4	N ·s/m	85.9			256.3
f_1	Hz	35	33	34	26
f_2	Hz	257		298	36
f_3	Hz				300
ξ_1		0.38	0.42	0.39	0.31
ξ_2		0.60		0.79	0.45
ξ_3					0.78

Note: The frequencies are undamped system frequencies.

Figure 3 illustrates comparisons of the predicted magnitude and phase of the impedance responses and the corresponding measured data for the new, 3-DOF, and 4-DOF models. The correlation coefficient (*r*-value) between each pair of data, used to judge goodness of the curve fit, is also shown in the figures. All the model predictions agree with the experimental data very well.

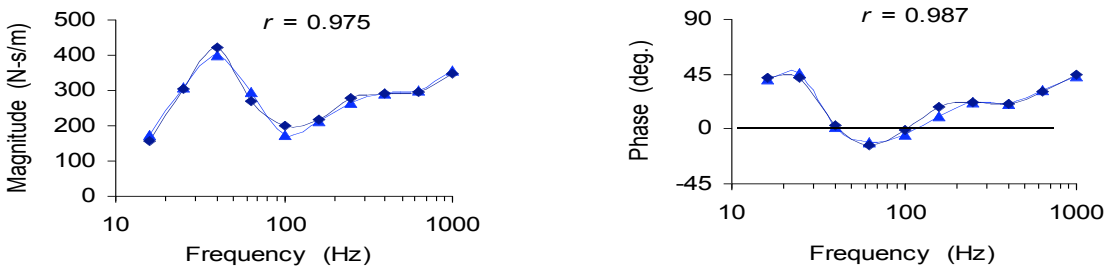

(a) New model

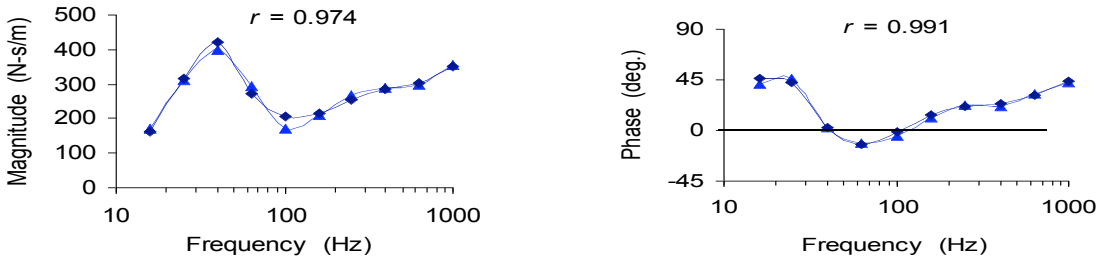

(b) 3-DOF Model

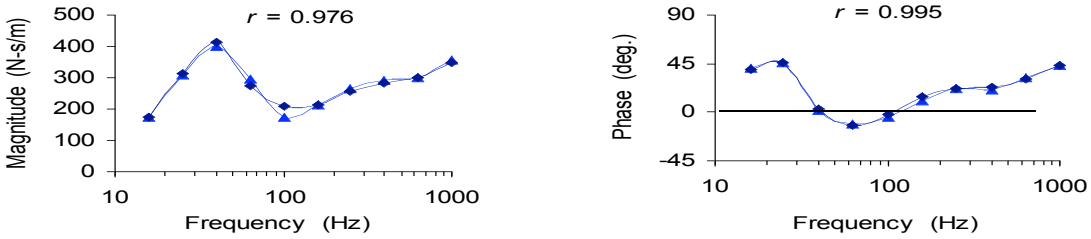

(c) 4-DOF mode

Figure 3: Comparisons of the experimental data (▲) and the predicted results (◆) of the (a) new, (b) 3-DOF, and (c) 4-DOF models.

Figure 4 shows comparisons of the predicted magnitude and phase of the impedance responses and the corresponding measured data, together with the comparison of the measured and predicted apparent mass magnitudes (Figure 4(c)). The error spectrum of the magnitude is also shown in Figure 4(d). The predicted impedance magnitude and phase responses show large differences from the experimental data at frequencies above 100 Hz. However, the predicted apparent mass agrees with the experimental data very well. The magnitude error of the apparent mass generally decreases with the increase in frequency.

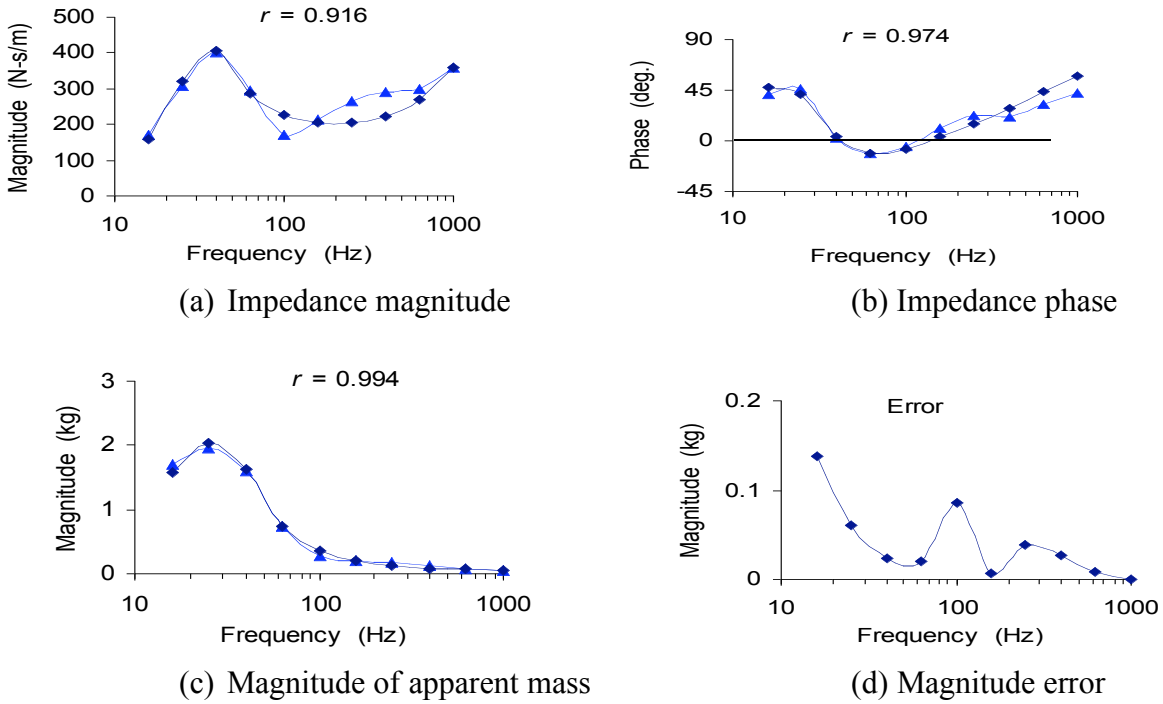

(a) Impedance magnitude (b) Impedance phase

(c) Magnitude of apparent mass (d) Magnitude error

Figure 4: Comparisons of the experimental data ( ) and the predicted results ( ) of the 2-DOF model and the magnitude error of the prediction.

Figure 5(a) shows the comparisons of the predicted finger vibration transmissibility from the new model and the reported experimental data (Kilhberg, 1995; Reynolds, 1977). The new model's transmissibility values at the wrist are shown in Figure 5(b).

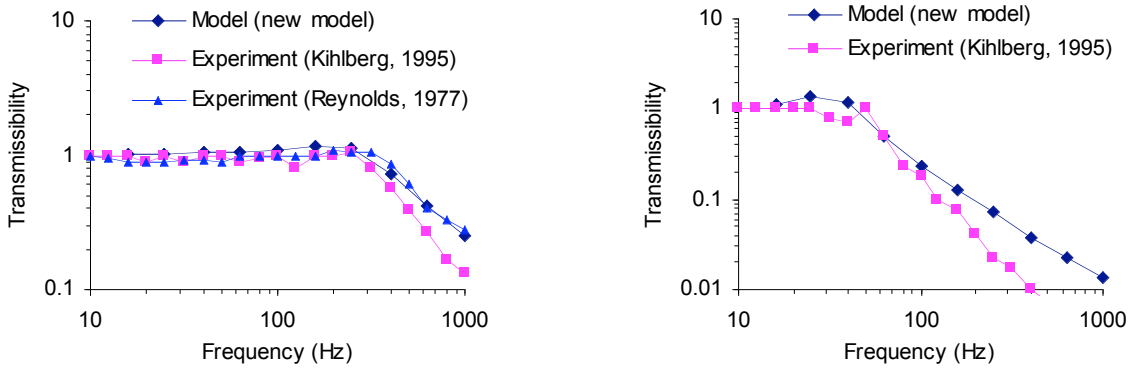

(a) Transmissibility at the fingers (b) Transmissibility at the wrist

Figure 5: Comparisons of the vibration transmissibility values predicted with the new model and the experimental data measured (a) at the fingers and (b) at the wrist.

Figure 6 shows the comparisons of the power absorption distributions predicted using the new model models. At frequencies ≤ 25 Hz, the power is primarily dissipated in the arm (c4). At frequencies ≥ 250 Hz, the power is mainly dissipated in the tissues near the hand contact area.

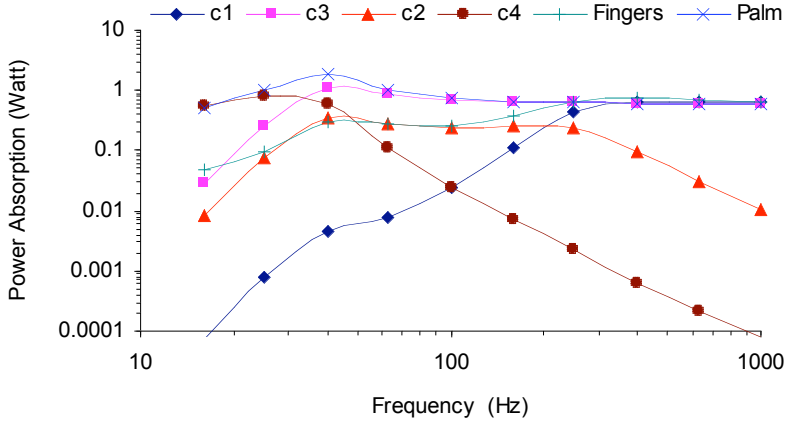

Figure 6: Distribution of the power absorption calculated using the new model.

4 DISCUSSION AND CONCLUSIONS

The highest natural frequency listed in Table 1 is similar to that estimated from $\sqrt{k_1/M_2}$ of the new model (= 253 Hz). This demonstrates that the finger resonance depends primarily on the effective mass of the fingers and finger contact stiffness. On the hand, the palm resonance depends mainly on the effective mass of the palm-wrist-forearm structure and the palm contact stiffness, since the estimated frequency of the new model ($\sqrt{k_3/M_4}$ = 32 Hz) is close to that listed in the table. Obviously, these resonances are associated with two different substructures of the hand gripping the handle. The 2-DOF model can reasonably reflect the palm resonance, but it cannot predict the finger resonance. The 3-DOF and 4-DOF models reflect all these resonant frequencies, but their high contact stiffness (k_1 >450 kN/m) does not appropriately represent any portion of the hand contact. This suggests that it is difficult to use a single-point coupling to simulate the distributed resonances. Some parameters of these models cannot be interpreted as the mechanical properties of any specific part of the hand and arm structures. Therefore, such models may be used to simulate the response but they may not provide a reasonable simulation of the hand and arm structure. These observations at least partially explain why some of the parameters of the reported models could be unrealistic.

The 4-DOF model reasonably simulates not only the response but also the hand and arm structures. Therefore, it is the best model for understanding the vibration transmission and power absorption in the system, for analyzing the interaction between the vibrating tool and the hand-arm system, and for constructing a general hand-arm simulator for tool and anti-vibration device tests. This model makes it possible to separately examine the isolation effectiveness of an anti-vibration device at the fingers and at the palm of the hand. More DOFs may be inserted between the ground and the forearm mass (M_4) of this model to more accurately simulate low frequency (<25 Hz) responses.

However, to build a hand-arm simulator for a tool test, it is not necessary to simulate the hand-arm structure. The criteria for such an application are as follows: (1) the model should provide a reasonable simulation of the driving-point biodynamic response in the major vibration direction of the tool; and (2) the model is feasible, practical, and inexpensive for the construction, adjustment, and operation of the simulator. The 2-DOF model is the simplest one that can provide a reasonable simulation of the response in a certain frequency range. The apparent mass is proportional to the dynamic force that can directly influence the tool dynamic behaviors. Probably for this reason, the mass of the tool vibration measurement accelerometer is limited to less than 5% of the tool mass (ISO 5349, 2001). If the tool mass is 1 kg, the accelerometer mass limitation is 50 g, which is actually larger than the apparent mass of the hand at frequencies above 500 Hz, as shown in Figure 4(c). The mass errors on the 2-DOF model at frequencies above 125 Hz are less than 50 g, as shown in Figure 4(d). The largest mass errors of the 2-DOF occur at the lower frequencies; they are comparable with those of the other models. Therefore, the 2-DOF may be suitable for the construction of a hand-arm simulator for tests of some large tools such as chipping hammers, rock drills, and road breakers.

5 REFERENCES

Dong, R.G., Rakheja, S., Schopper, A.W., Han, B., and Smutz, W.P., 2001. Hand-transmitted vibration and biodynamic response of the human hand-arm: a critical review. Critical Reviews™ in Biomedical Engineering 29, 391-441.

Dong, R.G., Welcome, D.E., McDowell, T.W., and Wu, J.Z., 2006. Measurement of Biodynamic Response of Human Hand-Arm System. Journal of Sound and Vibration 294, 807-827.

Dong, R.G., Wu, J.Z., McDowell, T.W., Welcome, D.E., Schopper, A.W., 2005. Distribution of mechanical impedance at the fingers and the palm of human hand. Journal of Biomechanics 38, 1165-1175.

Griffin, M.J., 1994. Foundations of hand-transmitted vibration standards, Nagoya Journal of Medical Science (Suppl.) 57, 147-164.

ISO8727, 1997. Mechanical vibration and shock - Human exposure-Biodynamic coordinate systems. Geneva, Switzerland: International Organization for Standardization.

ISO10819, 1996: Mechanical vibration and shock -- hand-arm vibration -- method for the measurement and evaluation of the vibration transmissibility of gloves at the palm of the hand. International Organization for Standardization, Geneva, Switzerland.

ISO10068, 1998: Mechanical vibration and shock -- free, mechanical impedance of the human hand-arm system at the driving point. International Organization for Standardization, Geneva, Switzerland.

Kihlberg, S., 1995. Biodynamic response of the hand-arm system to vibration from an impact hammer and a grinder. International Journal of Industrial Ergonomics 16, 1-8.

Rakheja, S., Wu, J.Z., Dong, R.G. and Schopper, A.W., 2002. A comparison of biodynamic models of the human hand-arm system for applications to hand-held power tools. Journal of Sound and Vibration 249, 55-82.

Reynolds, D.D., 1977. Hand-arm vibration: A review of 3 years research. Proceedings of the 2nd International Conference on Hand-Arm Vibration, Cincinnati, OH, USA, 99-128.